Princeton Plasma Physics Laboratory

PPPL- 4688

PPPL- 4688

ULF Wave Absorption at Mercury

Eua-Hwa Kim, Jay R. Johnson, and Kyung-Dong Lee

September, 2011

Prepared for the U.S. Department of Energy under Contract DE-AC02-09CH11466.

ULF wave absorption at Mercury

Eun-Hwa Kim,[1] Jay R. Johnson,[1] and Kyung-Dong Lee[2]

Received 24 June 2011; revised 27 July 2011; accepted 28 July 2011; published 30 August 2011.

[1] The field line resonance at Mercury is expected to occur when the ion-ion hybrid (IIH) and/or Alfvén resonance conditions are satisfied. However, the relative efficiency of wave energy absorption at these resonances has not been studied in the context of Mercury's magnetosphere. To understand the efficiency of wave absorption, we evaluate absorption coefficients at the IIH and Alfvén resonances for variable concentrations of sodium and azimuthal and field-aligned wave numbers in 1D multi-ion plasmas. The results show that wave absorption is much more efficient at the IIH resonance than at the Alfvén resonance at Mercury. Our results suggest that the mode conversion efficiency is sensitive to the azimuthal and field aligned wave numbers as well as heavy ion concentration ratio. Therefore, the radial profile of field-line resonances at Mercury can exhibit complex, discontinuous structure. **Citation:** Kim, E.-H., J. R. Johnson, and K.-D. Lee (2011), ULF wave absorption at Mercury, *Geophys. Res. Lett.*, *38*, L16111, doi:10.1029/2011GL048621.

1. Introduction

[2] Ultra-low frequency (ULF) waves in the ion gyrofrequency (ω_{ci}) range have been detected inside Mercury's magnetosphere during the 1st Mariner 10 flyby [*Russell*, 1989] and for both the 1st and 2nd MESSENGER flybys [*Boardsen et al.*, 2009a, 2009b]. The observed wave frequencies are comparable to ω_{ci} for both events from Mariner 10 and MESSENGER. Because observations showed that the region around Mercury is filled with heavy ions, such as Na^+, O^+, K^+ and He^+ [e.g., *Zurbuchen et al.*, 2008], waves at Mercury require a treatment that includes multiple ions with gyrofrequency effects [*Othmer et al.*, 1999; *Glassmeier et al.*, 2003; *Klimushkin et al.*, 2006; *Kim et al.*, 2008a].

[3] There have been several efforts to identify the observed ULF waves at Mercury. The first observed ULF waves at Mercury were believed to be a field-line resonance (FLR) standing mode along the magnetic field line [*Russell*, 1989] based on a single fluid plasma description. Later, *Othmer et al.* [1999] and *Klimushkin et al.* [2006] suggested that these waves were FLRs in multi-ion plasma and that the crossover frequency (ω_{cr}) is the preferred frequency for the FLR at Mercury.

[4] However, there also have been other interpretations. Unlike FLR at Earth, the signals from Mariner 10 were preferentially polarized in the magnetic meridian rather than the east-west direction and the observed waves also have strong field-aligned fluctuations. For these reasons *Blomberg* [1997] and *Southwood* [1997] argued that the observed waves could not be pure standing Alfvén waves. Waves detected by MESSENGER also have strong field-aligned magnetic components; therefore, *Boardsen et al.* [2009a] also suggested these waves are not standing modes.

[5] In multi-ion plasmas, wave absorption occurs at the Alfvén ($\omega < \omega_{c1}$) and/or ion-ion hybrid (IIH) resonances ($\omega_{c1} < \omega < \omega_{c2}$) [e.g., *Stix*, 1992; *Klimushkin et al.*, 2006; *Kim et al.*, 2008a]. *Kim et al.* [2008a] performed wave simulations in electron-proton-sodium plasmas and demonstrated that FLRs at Mercury should occur when the ion-ion hybrid (IIH) and/or Alfvén resonance conditions are satisfied. The simulation results also showed the magnetic field of FLRs at Mercury's magnetosphere oscillates linearly in the east-west meridian, which is similar to FLR at Earth.

[6] However, the detailed characteristics of FLR at Mercury have not been thoroughly investigated. In particular, the relative efficiency of wave energy absorption at the resonances has not been studied in the context of Mercury's magnetosphere.

[7] The aim of this letter is to determine the energy absorption at the IIH and/or Alfvén resonances and to predict how FLRs appear in Mercury's magnetosphere. To achieve these goals, we evaluate reflection, transmission and absorption coefficients for variable concentrations of sodium and azimuthal and field-aligned wave numbers.

2. Ion-Ion Hybrid and Alfvén Resonances

[8] When $\omega \ll \omega_{ce}, \omega_{pe}$, where ω_{ce} and ω_{pe} are the electron gyro- and plasma frequencies, the basic description of the plasma wave is given by the approximate cold plasma dispersion relation

$$n_\perp^2 \cong \frac{\left(r - n_\parallel^2\right)\left(l - n_\parallel^2\right)}{\left(s - n_\parallel^2\right)}, \quad (1)$$

where $n_\parallel$ and $n_\perp$ are refractive indices parallel and perpendicular to the ambient magnetic field ($\mathbf{B}_0$), respectively. For a two ion plasmas, the Stix function, r, l and s are [*Johnson et al.*, 1995]

$$\begin{pmatrix} r \\ l \end{pmatrix} \cong \pm \frac{c^2}{V_A^2} \frac{\omega_{c1}\omega_{c2}}{\omega_{cut}} \frac{(\omega \pm \omega_{cut})}{(\omega \pm \omega_{c1})(\omega \pm \omega_{c2})}, \quad (2)$$

$$s \cong \frac{c^2}{V_A^2} \frac{\omega_{c1}^2\omega_{c2}^2}{\omega_{bb}^2} \frac{\left(\omega^2 - \omega_{bb}^2\right)}{\left(\omega^2 - \omega_{c1}^2\right)\left(\omega^2 - \omega_{c2}^2\right)}, \quad (3)$$

where V_A and ω_{cut} are the Alfvén velocity and the cutoff frequency for $r = 0$ or $l = 0$, respectively. This approximate

[1] Princeton Plasma Physics Laboratory, Princeton University, Princeton, New Jersey, USA.
[2] Department of Astronomy and Space Science, Kyung Hee University, Yongin, South Korea.

0094-8276/11/2011GL048621

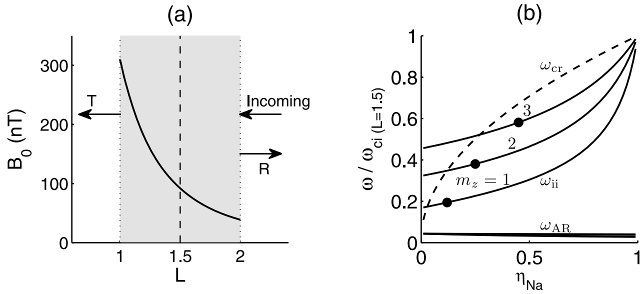

Figure 1. (a) The ambient magnetic field (B_0) in x. Here, the dashed line is the resonance location at L = 1.5. $\mathcal{R}$ and $\mathcal{T}$ are reflection and transmission coefficients, respectively. (b) The normalized Alfvén ($\omega_{\rm AR}$) and ion-ion hybrid resonance ($\omega_{\rm ii}$, solid) and crossover frequencies ($\omega_{\rm cr}$, dashed line) to $\omega_{\rm ci}$ at L = 1.5 for m_z = 1, 2, and 3.

dispersion relation has a resonance for perpendicular propagation $n_\perp \rightarrow \infty$ at

$$n_\parallel^2 = s, \tag{4}$$

and the cutoff conditions of $n_\perp \rightarrow 0$ at $n_\parallel^2 = r$ (l). In two fluid plasmas or below the heaviest ion gyrofrequency in multi-ion plasmas, this resonance is reduced to the Alfvén resonance (or the perpendicular ion cyclotron resonance) ($s \rightarrow c^2/V_A^2$) [*Karney et al.*, 1979; *Stix*, 1992]. The resonance can also be satisfied at higher frequency ($\omega_{\rm ii}$) between a pair of ion gyrofrequencies where $s(\omega_{\rm ii}) = n_\parallel^2(\omega_{\rm ii})$ and is known as the ion-ion hybrid (IIH) resonance. The IIH resonance is believed to have an important role for electromagnetic ion cyclotron wave generation near the equatorial region [*Lee et al.*, 2008] and energy transfer at the magnetopause (J. R. Johnson and E.-H. Kim, The effects of heavy ions on magnetopause mode conversion process, submitted to Journal of Geophysical Research, 2011).

3. Model Description

[9] In this study, we will examine how efficiently compressions are absorbed at the resonances as they propagate into the inner magnetosphere of Mercury. To address this problem, we consider a simplified 1D model that captures the essential features of the IIH and Alfvén resonances. Assuming radial propagation across field lines, we seek to understand how wave absorption depends on sodium concentration ratio, azimuthal and field-aligned wavenumber of the IIH wave mode. To isolate these effects we will consider wave absorption to occur at a particular field line which allows us to keep field gradients fixed.

[10] As an approximation to radial wave propagation across magnetic flux surfaces, we consider a cold plasma slab model. The slab model is a local approximation where x, y, and z correspond to radial, azimuthal, and field-aligned coordinates. Wave propagation in the cold, fluid model can be described by Maxwell's equations combined with fluid equations for ions and electrons. A simple set of linearized wave equations can be obtained by ignoring electron inertial effects and background gradients related to diamagnetic drift and density compressions (Johnson and Kim, submitted manuscript, 2011),

$$\frac{c}{\omega}\frac{\partial \mathbf{Y}}{\partial x} = \mathbf{MY}, \tag{5}$$

where

$$\mathbf{Y} = \begin{pmatrix} E_y \\ \dfrac{c}{\omega}\dfrac{\partial E_y}{\partial x} - in_yE_x \end{pmatrix}, \tag{6}$$

and

$$\mathbf{M} = \begin{pmatrix} \dfrac{n_yd}{n_z^2 - s} & 1 + \dfrac{n_y^2}{n_z^2 - s} \\ \dfrac{\left(n_z^2 - r\right)\left(n_z^2 - l\right)}{n_z^2 - s} & -\dfrac{n_yd}{n_z^2 - s} \end{pmatrix}, \tag{7}$$

where n_y is the refractive index in y and $d = (r - l)/2$. Equations (5)–(7) have been solved with a finite difference approach with nonuniform mesh [*Johnson*, 1992; *Johnson et al.*, 1995; Johnson and Kim, submitted manuscript, 2011].

[11] We adopt following assumptions to solve the wave equations at Mercury:

[12] 1. We model the region between L = 1 and 2 as shown in Figure 1a. Incoming waves are assumed to propagate from the lower magnetic field region (outer magnetosphere) and have a resonance at L = 1.5 as shown in Figure 1a. The wave solution is decomposed into WKB solutions at the boundaries to determine reflection, transmission, and absorption coefficients. For simplicity we assume $L_x = 2R_M$, $L_y = 2\pi \times 1.5R_M$, and L_z is the dipole field line length at L = 1.5 ($L_z = 0.93R_M$), where R_M is Mercury's radius. In order to calculate the resonant wave frequencies and wave solutions, azimuthal (k_y) and field-aligned (k_z) wavenumbers are assumed to be $k_y = m_yk_{y0}$, $k_z = m_zk_{z0}$, where $k_{y0} = 2\pi/L_y$, $k_{z0} = \pi/L_z$ (assuming the fundamental wavelength is $2L_z$), and m_y and m_z are azimuthal and field-aligned wave harmonic numbers, respectively.

[13] 2. The ambient magnetic field strength is $B_0 = B_s/L(x)^3$, where $B_s = 3.1 \times 10^{-7}$ T is the magnetic field strength at Mercury's surface [*Anderson et al.*, 2008]. Figure 1a shows the adopted magnetic field model and calculation boundaries.

[14] 3. The electron density ($N_{\rm e}$) is assumed to be a constant and has a typical value of $N_{\rm e}$ = 3 cm^{-3} [*Russell*, 1989]. Because sodium ions are one of the main constituents at Mercury [e.g., *Ip*, 1986; *Cheng et al.*, 1987; *Zurbuchen et al.*, 2008], we adopt an electron-proton-sodium plasma in our model. The sodium ion density ratio $\eta_{\rm Na} = N_{\rm Na}/N_{\rm ion}$, where $N_{\rm ion}$ is the ion number density, is assumed to be a constant in x.

[15] To examine how the resonance condition depends on $\eta_{\rm Na}$ and m_z, we compute the Alfvén ($\omega_{\rm AR}$) and ion-ion hybrid ($\omega_{\rm ii}$) frequencies that satisfy the resonance condition ($s = n_\parallel^2$) at L = 1.5. Figure 1b shows $\omega_{\rm AR}$ and $\omega_{\rm ii}$ as a function of $\eta_{\rm Na}$ for m_z = 1, 2, and 3. Figure 1b clearly shows that $\omega_{\rm ii}$ increases and $\omega_{\rm AR}$ decreases as $\eta_{\rm Na}$ increases. Because $\omega_{\rm AR}$ harmonics are smaller than the heaviest ion gyrofrequency, $\omega_{\rm AR} < \omega_{\rm cNa} = 0.045\omega_{\rm ci}$, higher harmonics of $\omega_{\rm AR}$ are close to the fundamental. In contrast to $\omega_{\rm AR}$, $\omega_{\rm ii}$ exhibits distinct harmonic structure.

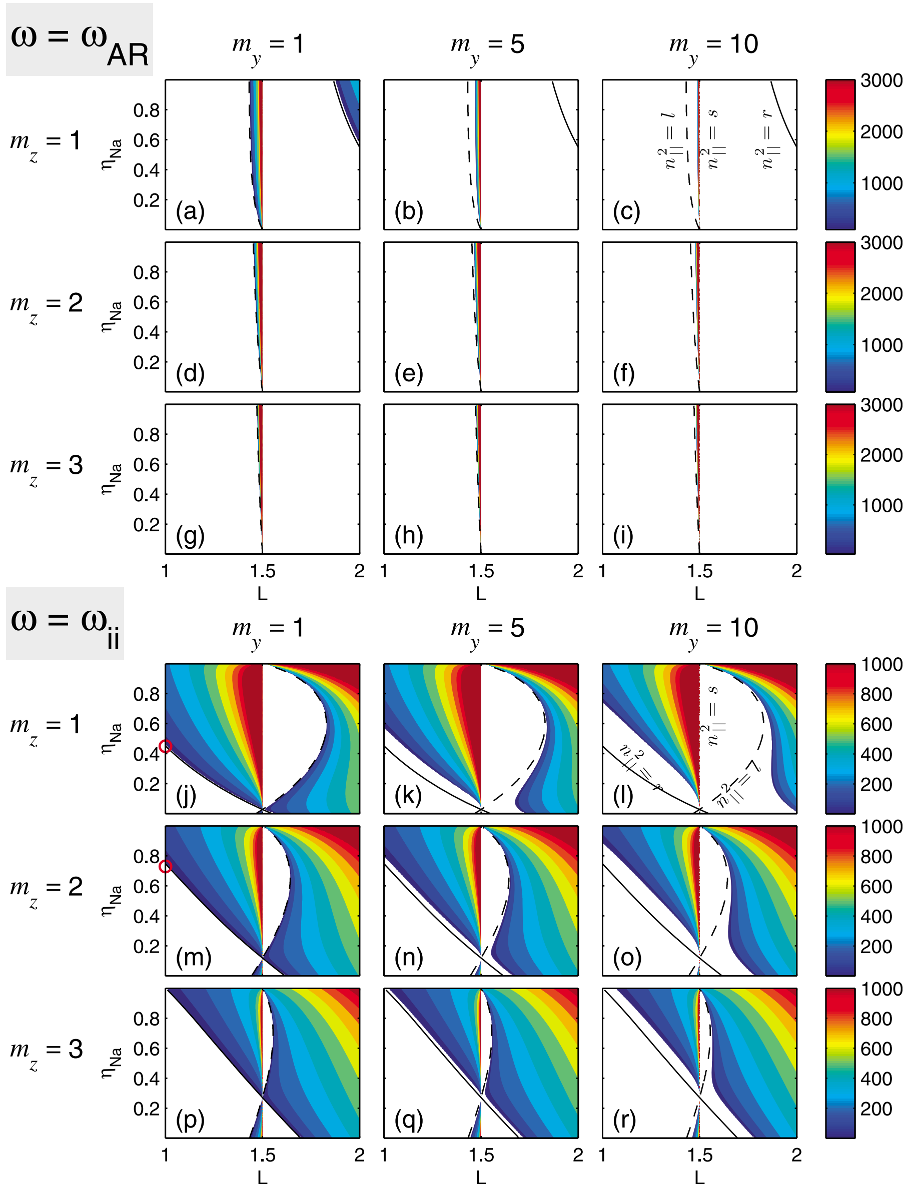

Figure 2. The refractive index n_x of incoming compressional waves for (a–i) $\omega = \omega_{AR}$ and (j–r) $\omega = \omega_{ii}$ at $L = 1.5$ for different m_y and m_z. Here horizontal and vertical axes are L and η_{Na}. Black solid and dashed lines are cutoff conditions for $n_y = 0$ ($n_\parallel^2 = r$ (l)) and red circles in Figures 2j and 2m are η_{Na}^{min} where $n_x = 0$ at $L = 1$.

[16] In between two ion gyrofrequencies, there is a special frequency where $r = l = s$ and $d = 0$, called the crossover frequency, $\omega_{cr}^2 = \eta_1\omega_{c2}^2 + \eta_2\omega_{c1}^2$. In Figure 1b, we plot ω_{cr} as a dashed line. Here we define η_{cr}, where $\omega = \omega_{cr}$, and $\eta_{cr} = 0.3$, 0.12 and 0.27 for $m_z = 1$, 2, and 3, respectively.

[17] After we calculate the wave frequency satisfying the resonance condition at $L = 1.5$ for a given η_{Na} and m_z, the refractive index and wave solutions in x are derived for different azimuthal mode number m_y.

4. Dispersion Relation

[18] The refractive index $n_x = ck_x/\omega$ of incoming compressional waves along x are calculated as a function of m_y and η_{Na} for $m_z = 1, 2,$ and 3. Figure 2 shows n_x for $\omega = \omega_{AR}$ and $\omega = \omega_{ii}$. In Figure 2, blank areas represent wave stop gaps. The boundaries of the wave stop gaps show a resonance at $L = 1.5$ or cutoffs with $n_x^2 = (r - n_z^2)\,(l - n_z^2)/(s - n_z^2) - n_y^2 = 0$.

[19] For $\omega = \omega_{AR}$ in Figures 2a–2i, waves can only propagate in a narrow region near $L = 1.5$ except $(m_y, m_z) = (1,1)$ in Figure 2a. When m_y and/or m_z increase, both cutoffs move to the outer magnetosphere (lower magnetic field region) and wave propagation regions become narrower in x. In Figure 2a, for $\eta > 0.58$ incoming waves are partially reflected at the outer cutoff near $n_z^2 = r$ and encounter the resonance at $L = 1.5$. However, in Figures 2b–2f, $n_x^2 < 0$ at $L = 2$ and no wave can propagate toward the resonance.

[20] In contrast to the Alfvén resonance case, for $\omega = \omega_{ii}$ in Figures 2j–2r, $n_x^2 > 0$ at $L = 2$ and all incoming waves propagate in the inhomogeneous plasma region. For the case of small m_y shown in Figures 2j, 2m, and 2p, there is a particular $\eta = \eta_{cr}$ where the resonance and two cutoffs almost match

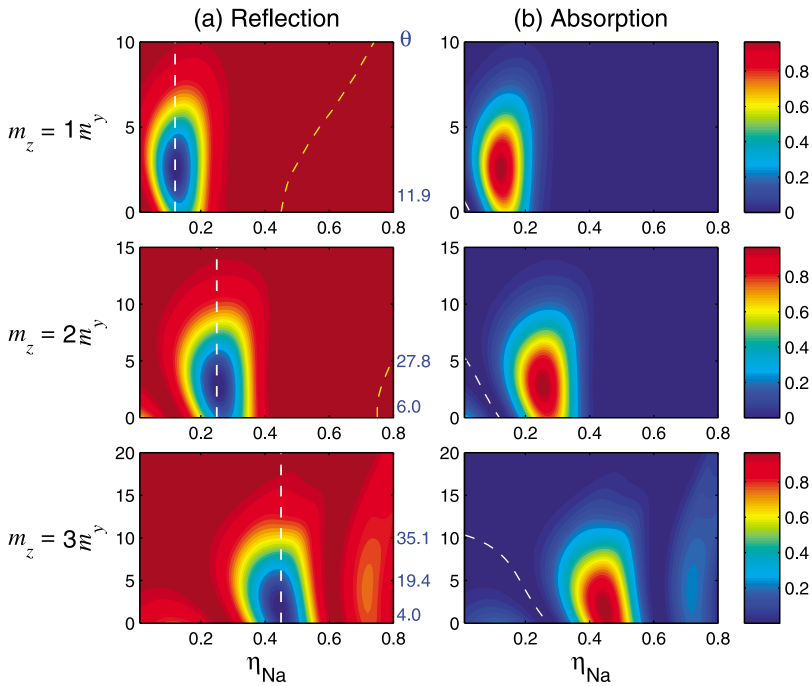

Figure 3. (a) Reflection ($\mathcal{R}$) and (b) absorption ($\mathcal{A}$) coefficients at the IIH resonance as a function of η_{Na}, m_y, and m_z. The white and yellow dashed lines in (a) are η_{Na}, where $\mathcal{A}$ has the maximum value, and η_{Na}^{min}, where $n_x = 0$, respectively. The white dashed lines in Figure 3b show the location with no absorption from equation (8). Here $\theta = \tan^{-1}(k_y/k_z)$.

each other. This is the crossover location where $\omega = \omega_{cr}$. It is noted that for $\eta = \eta_{cr}$ and $m_y = 0$, equation (7) reduces to $(c^2/\omega^2)\,E''_y + (n_\parallel^2 - s)\,E_y = 0$ and the waves are decoupled [e.g., *Klimushkin et al.*, 2006]. For $m_y \neq 0$, wave coupling between incoming compressional wave and IIH resonance can occur. Outer cutoffs in the lower magnetic field region occur near $n_\parallel^2 = l$ for $\eta_{Na} < \eta_{cr}$ and $n_\parallel^2 = r$ for $\eta_{Na} > \eta_{cr}$.

[21] For $\eta_{Na} > \eta_{cr}$, there is a minimum sodium concentration, η_{Na}^{min} at $L = 1$, where the wave cannot propagate ($n_x^2 = 0$) indicated with red circles in Figures 2j and 2m. For $\eta_{Na} < \eta_{Na}^{min}$, waves reflect prior to reaching the inner boundary at $L = 1$ and there is a cutoff-resonance-cutoff triplet. In this case absorption at the IIH resonance can occur both as the wave leaks through the resonance as well as when the wave reflects off the inner cutoff and propagates back into the resonance where the largest absorption can occur. Superposition of the incoming and reflected wave near the resonance can lead to larger absorption than the 25% Budden limit of the cutoff-resonance pair [*Lee et al.*, 2008]. Thus the wave absorption can be as large as 100%. For $\eta_{Na} > \eta_{Na}^{min}$, the waves propagate out of the inner boundary of the domain and there is transmission.

5. Wave Absorption at the Ion-Ion Hybrid Resonance

[22] We calculate wave absorption ($\mathcal{A}$), reflection ($\mathcal{R}$), and transmission ($\mathcal{T}$) coefficients for Mercury's magnetosphere. For $\omega = \omega_{AR}$ in Figure 2, most waves cannot propagate into the resonance and there is little absorption (the maximum of $\mathcal{A}$ at the Alfvén resonance is 6% for (m_y, m_z) = (1, 1)) and there is very little structure in the coefficients. Therefore, we focus primarily on the coefficients for the case where $\omega = \omega_{ii}$. Because $\mathcal{T}$ is small, we only show $\mathcal{A}$ and $\mathcal{R}$ in Figure 3. The results are summarized below.

[23] The maximum values of $\mathcal{A}$ ($\mathcal{A}_{max}$) are up to 100% for all m_z cases. In Figure 3a, we have shown η_{Na}^{min} as yellow dashed lines, and most wave absorption occurs in relatively low sodium density ($\eta_{Na} < \eta_{Na}^{min}$). As we described in Section 4, in this region of η_{Na}, waves encounter a cutoff-resonance-cutoff triplet and there is no transmission.

[24] The values of η_{Na}, where $\mathcal{A} = \mathcal{A}_{max}$, increase as m_z increases. For instance, $\mathcal{A}_{max}$ occurs at η_{Na} = 0.12, 0.25, and 0.45 for m_z = 1, 2, and 3, respectively, as marked as white dashed lines in Figure 3a. Because ω_{ii} increases as η_{Na} increases, η_{Na} for each m_z can be converted to the incoming wave frequencies (See Figure 1b). Wave frequencies where $\mathcal{A} = \mathcal{A}_{max}$ at (η_{Na}, m_z) = (0.12, 1), (0.25, 2), and (0.45, 3) are 0.2, 0.4, and 0.6 ω_{ci}, respectively. Thus wave frequencies with higher field-aligned harmonic numbers have strong absorption when the plasma contains a higher concentration of heavy ions.

[25] The value of m_y where $\mathcal{A} = \mathcal{A}_{max}$ is almost the same for different m_z values, but the width of the m_y absorption window ($\triangle m_y$) becomes wider as m_z increases. For instance, at η_{Na} ($\mathcal{A} = \mathcal{A}_{max}$), $\triangle m_y \sim$ 10, 14, and 17, for m_z = 1, 2, and 3, respectively. However, $\mathcal{A}_{max}$ occurs at m_y = 2–3 for all m_z cases.

[26] The absorption oscillates in η_{Na}. The first minimum can be analytically examined. *Stix* [1992] estimated that the energy absorption coefficient $\mathcal{A}$ at the Alfvén or IIH resonance is proportional to

$$\mathrm{Ai}(0)\sigma + \mathrm{Ai}'(0)\left(1 + \sigma\nu^2\right), \qquad (8)$$

where $\sigma = \alpha + \beta/\nu^2$, $\alpha = (d^2 - n_y d')\,(T')^{-4/3}$, $\beta = -n_y\,(T')^{-1}$, $\nu = n_y\,(T')^{-1/3}$ and $T = s - n_z^2 - n_y^2$. From equation (8), we derive n_y^0

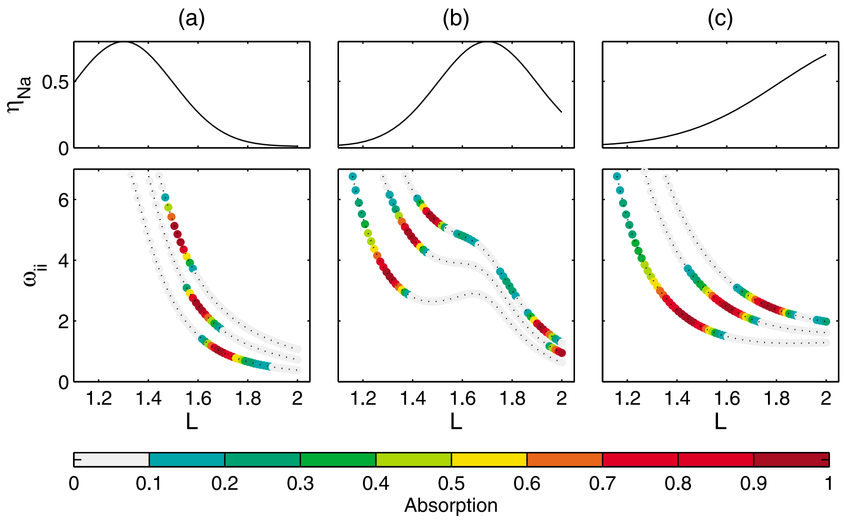

Figure 4. (a–c) Three harmonics of $\omega_{\rm ii}$ for different $\eta_{\rm Na}$ profile in radial direction. Different color represents the absorption at each wave frequency in $\eta_{\rm Na}$.

where $\mathcal{A}$ = 0 and plot as a white, dashed line in Figure 3b. Here both analytic and numerical results show $\mathcal{A} \rightarrow 0$ when $n_y^0 \rightarrow 0$ at $\eta_{\rm Na} = \eta_{\rm cr}$. For $n_y \neq 0$, the analytical approximations also show good agreement with our numerical results. This comparison is reasonable as large as the cutoff-resonance-cutoff triplet are close together (much less than a wavelength). For larger m_y, however, it is expected that the analytic approximation is not as accurate. However, in this case the absorption vanishes independent of $\eta_{\rm Na}$ at large m_y. Therefore, there is no meaning to compare the numerical and analytical results. But for small $\theta = \tan^{-1}(k_y/k_z) \leq 10°$, the two solutions match well each other (Johnson and Kim, submitted manuscript, 2011). Oscillation in the large $\eta_{\rm Na}$ region can be explained as the result of interference between incoming and reflected waves near the resonance. A similar interference effect between incoming and reflected Langmuir waves leading to oscillations in mode conversion efficiency was also found at higher frequency (near the electron plasma frequency) [*Kim et al.*, 2008b].

6. Discussion and Conclusion

[27] In this letter, resonant wave absorption at the IIH resonance is computed to investigate the FLR at Mercury. First, we found that the absorption at the Alfvén resonance can only occur for a limited range of parameters (m_y, m_z and $\eta_{\rm Na}$) as shown in Figure 2 and is not particularly efficient at Mercury. In contrast, absorption at the IIH resonance occurs for a much broader range of parameters and is much more efficient. Second, the absorption at the IIH resonance is very sensitive to wave number and the ion concentration ratio. Details of the absorption at IIH resonance are: (1) The maximum values of absorption can be as large as 100%; (2) The values of $\eta_{\rm Na}$, where $\mathcal{A}$ has a maximum, increases as m_z increases; (3) The value of m_y, where $\mathcal{A}$ has a maximum is almost the same for different m_z values, but the m_y width of the absorption window becomes wider as m_z increases; and (4) When m_z increases, $\mathcal{A}$ oscillates as a function of $\eta_{\rm Na}$.

[28] At Earth's magnetosphere, when heavy ions are included, FLR radial structure can be smooth [*Fraser et al.*, 2005]. Our results suggest that the radial structure of FLRs at Mercury is more sensitive to wave harmonic numbers and the heavy ion density ratio profile than at Earth. Figure 4 shows an example of three different profiles of sodium concentration. In each case, the resonant harmonic frequencies are shown as dotted lines in Figure 4. Ignoring the dependence on the magnetic field gradient and magnetic field line length, we show the expected absorption level at each radial position as a function of $\eta_{\rm Na}$. When $\eta_{\rm Na}$ decreases in L in Figure 4a, the maximum absorption frequency also decreases. Because higher harmonic waves have stronger absorption, the observed FLR profile in L is expected to have sharper structure than the normal $\omega_{\rm ii}$ profile. However, in Figure 4b for $L < 1.5$, $\omega_{\rm ii}$ shows a distinct structure, and the maximum absorption frequency increases in L. It also shows a discontinuous structure in L. For the last case in Figure 4c, the observed FLR frequency could be independent of L and in the range of ω = 2–2.5 Hz.

[29] In this study, we examined the absorption at a single field line. Because each field line has different length, the wave number also changes in L. In addition, our results show that the absorption is sensitive to field-aligned wave number. Therefore in order to discuss the FLR radial profile more completely, it would be necessary to also investigate the absorption for different L shell (e.g., magnetic field gradients).

[30] In conclusion, we examined how efficiently wave absorption at IIH and Alfvén resonances operates in Mercury's magnetosphere. The results show that wave absorption is much more efficient at the IIH resonance than at the Alfvén resonance. Absorption coefficients are sensitive to the azimuthal and field aligned wave numbers as well as heavy ion concentration ratio. Our results suggest that the field-line resonances can have complex radial structure depending on heavy ion density and azimuthal wave numbers at Mercury.

[31] **Acknowledgments.** This work was supported by NASA grants (NNG07EK69I, NNH07AF37I, NNH09AM53I, NNH09AK63I, and NNH11AQ46I), NSF grant ATM0902730, and DOE contract DE-AC02-09CH11466.

[32] The Editor thanks Dmitri Klimushkin and Karl-Heinz Glassmeier for their assistance in evaluating this paper.

References

Anderson, B. J., M. H. Acuña, H. Korth, M. E. Purucker, C. L. Johnson, J. A. Slavin, S. C. Solomon, and R. L. McNutt (2008), The structure of Mercury's magnetic field from MESSENGER's first flyby, *Science*, *321*,82–85, doi:10.1126/science.1159081.

Blomberg, L. G. (1997), Mercury's magnetosphere, exosphere and surface: Low-frequency field and wave measurements as a diagnostic tool, *Planet. Space Sci.*, *45*, 143–148.

Boardsen, S. A., B. J. Anderson, M. H. Acuña, J. A. Slavin, H. Korth, and S. C. Solomon (2009a), Narrow-band ultra-low-frequency wave observations by MESSENGER during its January 2008 flyby through Mercury's magnetosphere, *Geophys. Res. Lett.*, *36*, L01104, doi:10.1029/2008GL036034.

Boardsen, S. A., J. A. Slavin, B. J. Anderson, H. Korth, and S. C. Solomon (2009b), Comparison of ultra-low-frequency waves at Mercury under northward and southward IMF, *Geophys. Res. Lett.*, *36*, L18106, doi:10.1029/2009GL039525.

Cheng, A. F., R. E. Johnson, S. M. Krimigis, and L. J. Lanzerotti (1987), Magnetosphere, exosphere, and surface of Mercury, *Icarus*, *71*, 430–440, doi:10.1016/0019-1035(87)90038-8.

Fraser, B. J., J. L. Horwitz, J. A. Slavin, Z. C. Dent, and I. R. Mann (2005), Heavy ion mass loading of the geomagnetic field near the plasmapause and ULF wave implications, *Geophys. Res. Lett.*, *32*, L04102, doi:10.1029/2004GL021315.

Glassmeier, K.-H., P. N. Mager, and D. Y. Klimushkin (2003), Concerning ULF pulsations in Mercury's magnetosphere, *Geophys. Res. Lett.*, *30*(18), 1928, doi:10.1029/2003GL017175.

Ip, W.-H. (1986), The sodium exosphere and magnetosphere of Mercury, *Geophys. Res. Lett.*, *13*, 423–426.

Johnson, J. R. (1992), Excitation of low frequency turbulence along auroral field lines, Ph.D. thesis, Mass. Inst. of Technol., Cambridge.

Johnson, J. R., T. Chang, and G. B. Crew (1995), A study of mode conversion in an oxygen-hydrogen plasma, *Phys. Plasmas*, *2*, 1274–1284.

Karney, C. F. F., F. W. Perkins, and Y.-C. Sun (1979), Alfven resonance effects on magnetosonic modes in large tokamaks, *Phys. Rev. Lett.*, *42*, 1621–1624, doi:10.1103/PhysRevLett.42.1621.

Kim, E.-H., J. R. Johnson, and D.-H. Lee (2008a), Resonant absorption of ULF waves at Mercury's magnetosphere, *J. Geophys. Res.*, *113*, A11207, doi:10.1029/2008JA013310.

Kim, E.-H., I. H. Cairns, and P. A. Robinson (2008b), Mode conversion of Langmuir to electromagnetic waves at magnetic field-aligned density inhomogeneities: Simulations, theory, and applications to the solar wind and the corona, *Phys. Plasmas*, *15*, 102110, doi:10.1063/1.2994719.

Klimushkin, D. Y., P. N. Mager, and K.-H. Glassmeier (2006), Axisymmetric Alfvén resonances in a multi-component plasma at finite ion gyrofrequency, *Ann. Geophys.*, *24*, 1077–1084.

Lee, D.-H., J. R. Johnson, K. Kim, and K.-S. Kim (2008), Effects of heavy ions on ULF wave resonances near the equatorial region, *J. Geophys. Res.*, *113*, A11212, doi:10.1029/2008JA013088.

Othmer, C., K.-H. Glassmeier, and R. Cramm (1999), Concerning field line resonances in Mercury's magnetosphere, *J. Geophys. Res.*, *104*, 10,369–10,378, doi:10.1029/1999JA900009.

Russell, C. T. (1989), ULF waves in the Mercury magnetosphere, *Geophys. Res. Lett.*, *16*, 1253–1256.

Southwood, D. J. (1997), The magnetic field of Mercury, *Planet. Space Sci.*, *45*, 113–117.

Stix, N. (1992), *Waves in Plasmas*, Am. Inst. of Phys., New York.

Zurbuchen, T. H., et al. (2008), MESSENGER observations of the composition of Mercury's ionized exosphere and plasma environment, *Science*, *321*, 90–92, doi:10.1126/science.1159314.

J. R. Johnson and E.-H. Kim, Princeton Plasma Physics Laboratory, Princeton University, PO Box 0451, Princeton, NJ 08543-0451, USA. (ehkim@pppl.gov)

K.-D. Lee, Department of Astronomy and Space Science, Kyung Hee University, Yongin, Gyeonggi 446-701, South Korea.

The Princeton Plasma Physics Laboratory is operated
by Princeton University under contract
with the U.S. Department of Energy.

Information Services
Princeton Plasma Physics Laboratory
P.O. Box 451
Princeton, NJ 08543

Phone: 609-243-2245
Fax: 609-243-2751
e-mail: pppl_info@pppl.gov
Internet Address: http://www.pppl.gov